Tribology Transactions

ISSN: 1040-2004 (Print) 1547-397X (Online) Journal homepage: https://www.tandfonline.com/loi/utrb20

A Hybrid Method for the Segmentation of a Ferrograph Image Using Marker-Controlled Watershed and Grey Clustering

Jingqiu Wang, Panpan Yao, Wanlong Liu & Xiaolei Wang

TRIBOLOGY TRANSACTIONS
2016, VOL. 59, NO. 3, 513–521
http://dx.doi.org/10.1080/10402004.2015.1091534

A Hybrid Method for the Segmentation of a Ferrograph Image Using Marker-Controlled Watershed and Grey Clustering

Jingqiu Wang[a,b], Panpan Yao[a], Wanlong Liu[a], and Xiaolei Wang[a,b]

[a]College of Mechanical and Electrical Engineering, Nanjing University of Aeronautics and Astronautics, Nanjing, China; [b]Jiangsu Key Laboratory of Precision and Micro-Manufacturing Technology, Nanjing, China

ABSTRACT
Aimed at the correct segmentation of wear particles in ferrograph images, a new method combining marker-controlled watershed and an improved grey clustering algorithm is proposed in this article. First, the marker-controlled watershed is applied to ferrograph images to efficiently obtain the initial segmentation of wear particles. Then, an improved grey clustering algorithm utilizing color characteristics and relative position information is applied to merge the oversegmented regions after the watershed segmentation. This new algorithm is tested for ferrograph images and the results are compared with those of other algorithms. The experimental results show that the proposed method is effective for the segmentation of large wear particles and fine wear debris deposited as chains on the ferrograph, and it is proven to be a practical method for segmenting wear particles quickly and accurately.

ARTICLE HISTORY
Received 22 October 2014
Accepted 1 September 2015

KEYWORDS
Wear particle analysis; ferrography; wear particle segmentation; marker-controlled watershed; grey clustering

Introduction

Ferrography was developed in the 1970s as a wear condition monitoring and fault diagnosis technology (Roylance *(1)*). It separates wear debris from a lubricant and deposits it on a transparent substrate and then determines the wear condition and failure mechanisms of the equipment through quantitative and qualitative analyses of the size, shape, and color features of wear particles (Laghari, et al. *(2)*; Wu, et al. *(3)*). Ferrography has been proved to be efficient for examining large particles, which is extremely important for engines, transmissions, and mining equipment (Roylance *(1)*; Eliaz and Latanision *(4)*; Cao, et al. *(5)*; Zhang, et al. *(6)*).

In recent years, improved methods for automatic processing and analysis of wear particle samples has been actively pursued (Peng and Goodwin *(7)*; Wang and Wang *(8)*), and ferrography has evolved to be more intelligent and automatic with the development of computer image processing and analysis techniques to decrease the dependence on human expertise (Stachowiak, et al. *(9)*; Stachowiak and Podsiadlo *(10)*; Surapol *(11)*; Wang, et al. *(12)*; Wu, et al. *(13)*; Peng *(14)*).

Figure 1 shows typical ferrograph images obtained by an optical microscope. Because the wear particles are deposited on the glass substrate using a gradient magnetic field, the ferro-particles usually distribute in the form of chains, which may contain a number of fine wear debris or some large wear particles, such as severe sliding or fatigue particles. Usually, severe wear generates wear particles larger than 15 μm. The presence of a number of large particles indicates a severe wear condition; thus, the detection of large particles is important in ferrograph analysis.

As shown in Fig. 1, the particles may be connected and even overlap, depending on the concentration. In addition, the complex morphology (shape, color, and surface texture), blurs edges because of the limited focus depth of the optical microscope, and the inhomogeneous image background color may lead to difficulties in computer-aided ferrography analysis.

Therefore, a method to effectively segment wear particles, particularly the large particles within deposited chains to facilitate further parameter extraction and type identification, is the key issue for the current computer-based intelligent ferrograph image analysis. As far as we know, there is no image segmentation algorithm that can be used to separate wear particles completely and successfully.

The watershed algorithm proposed by Vincent and Soille *(15)* is an important image segmentation method. It has been widely used in many fields, including medical image segmentation, because of its simplicity, high speed, and continuous edges (Nallaperumal, et al. *(16)*; Grau, et al. *(17)*).

However, because the watershed algorithm is sensitive to noise and regional extremes, oversegmentation is inevitable when it is applied to the segmentation of ferrograph images because of the complex morphology and surface texture of wear particles, especially large wear particles. To solve the oversegmentation problem, researchers have been seeking hybrid methods that combine the watershed algorithm with other segmentation methods.

Yang, et al. *(18)* proposed an image segmentation method based on watershed and ant colony clustering. First, the image was segmented with the watershed algorithm. Then, ant colony

CONTACT Xiaolei Wang wxl@nuaa.edu.cn
Color versions of one or more of the figures in the article can be found online at www.tandfonline.com/utrb.
Review led by Jack Poley

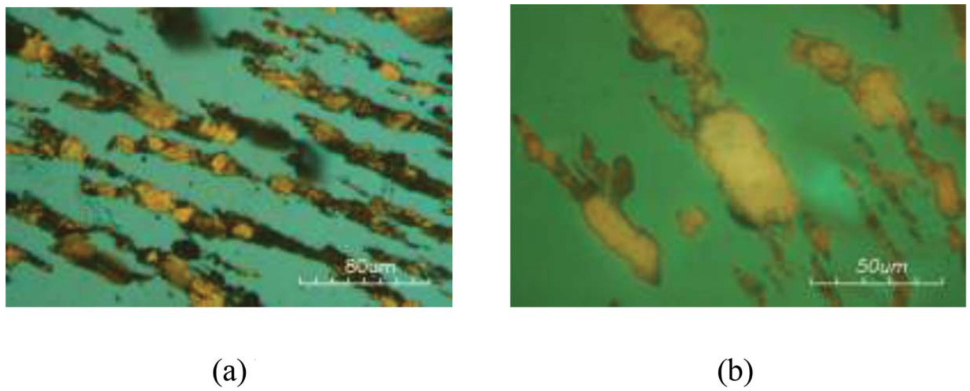

Figure 1. Typical ferrograph images: (a) wear particle chains and (b) large wear particles with blurred edges.

clustering was used to merge different regions of homogeneity, resulting in segmentation of medical images. Monteiro *(19)* proposed a framework of image segmentation that combines edge- and region-based information with spectral techniques through the morphological algorithm of watersheds. An initial partitioning of the image into primitive regions results from the application of a rain falling watershed algorithm on the image gradient magnitude. This initial partition is an input to a computationally efficient region segmentation process that produces the final segmentation. In our previous work (Wang, et al. *(20)*), a method that combined watershed and ant colony algorithm was tested. It was proven that such a hybrid method is effective for the segmentation of wear particles.

In 1982, Deng *(21)* developed grey theory, which focuses on problems with small samples and poor information. The system was named from the use of grey as the color indicating the amount of known information in control theory. In general terms, grey designates the uncertainty in less data and incomplete information. Thus, the grey system indicates that part of the information is clear, whereas part is still unknown.

Grey theory has been widely used in many fields, including automatic feature identification (Peng and Kirk *(22)*) and wear failure diagnosis (Chen, et al. *(23)*). In 1993, Huang and Wu *(24)* introduced the grey theory into image processing applications for image compression. After nearly 20 years of continuous efforts and exploration by researchers, progress has been made in the application of grey theory in image engineering, including image edge detection, image compression, image denoising, and image segmentation evaluation (Feng, et al. *(25)*; Ma, et al. *(26)*; He, et al. *(27)*). In these applications, the experimental images include natural images, medical images, and infrared images.

Inspired by the above studies, a new segmentation method for ferrograph images is proposed by combining marker-controlled watershed and grey clustering (CMWGC). First, the marker-controlled watershed algorithm is adopted to determine the initial segmentation of wear particles. Then, an improved grey clustering algorithm is proposed to merge the oversegmented regions to obtain accurate segmentation of wear particles, especially large wear particles such as severe sliding and fatigue particles. The segmentation methods are subsequently evaluated using real ferrograph images.

The proposed CMWGC algorithm

Initial segmentation of wear particles based on the marker-controlled watershed algorithm

The watershed transform, a popular segmentation method from the field of mathematical morphology, considers an image as a surface of mountainous terrain, and the grey level of each pixel denotes the altitude of that point. This terrain has deep valleys (minima), high ridges (watershed lines), and steep or gentle hillsides (catchment basins).

The traditional watershed algorithm is usually implemented by simulating a flooding process, as shown in Fig. 2. First, holes are pierced in each minimum; then, starting from the minimum of lowest altitude, water will progressively fill up the different catchment basins. At the points where water from different minima would merge, a “dam” is built to prevent intermingling. At the end of the flooding procedure, each minimum is completely surrounded by dams that delimit its associated catchment basins. All of the dams correspond to the needed watersheds.

In the segmentation process, the watershed algorithm has two main steps: sorting and flooding. First, all pixels are sorted in ascending order according to their grey values. Pixels of the same grey value can be directly accessed simultaneously. Once the pixels have been sorted, the progressive flooding can be processed from the minimal grey level. After a series of mergers and a new catchment construction process, segmentation of the image is achieved.

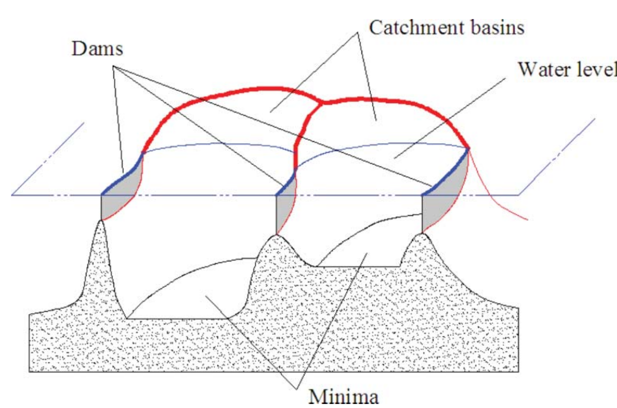

Figure 2. Schematic of the watershed algorithm.

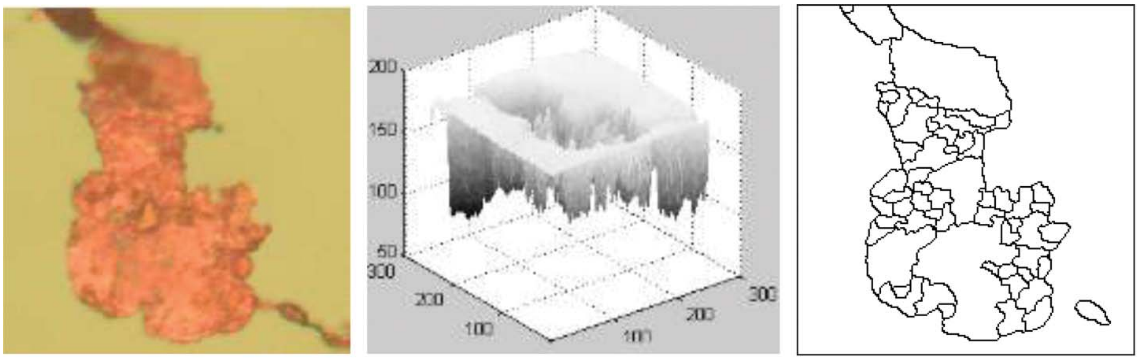

(a) (b) (c)

Figure 3. Fatigue particle and the result of watershed segmentation: (a) original image, (b) topographical diagram, and (c) final watershed segmentation.

Compared to other algorithms, the watershed algorithm is not affected by edges with poor contrast, so it guarantees closed and continuous edges. However, due to sensitivity to noise and regional minima, the watershed transform result contains a myriad of small regions when it infers catchment basins from gradient images, which makes this result useless. The use of a marker image (Vincent *(28)*) to reduce the number of minima of the image and thus the number of regions is the most commonly used solution. However, when the marker-controlled watershed algorithm is applied to ferrograph images, oversegmentation often occurs because of complex morphology features such as rough/irregular texture, color variation, and brightness change on the surface of some wear particles.

For example, Fig. 3a shows an original ferrograph image that has a large fatigue wear particle. Fatigue wear particles frequently have holes and folds on the surface that appear as a large number of minima in the grey topographical image, as shown in Fig. 3b. Therefore, the fatigue wear particle is unfortunately oversegmented as shown in Fig. 3c.

Figure 4a shows an original ferrograph image that has wear particle chains and black oxide particles. The marker-controlled watershed algorithm can separate the wear particles from the image background and a wear particle from the chains. However, for the large wear particles shown in the rectangular areas in Fig. 4b, oversegmentation occurs because of the inconsistent brightness on the surface of wear particles.

Region merging based on improved grey clustering

Grey relational analysis is a tool for analysing the relationships between one reference sequence and the other comparative ones in a given set. Grey relational analysis can be viewed as a measure of similarity for different sequences (Chang and Yeh *(29)*).

Assume that the reference sequence is defined as $X_0 = (x_0(1), x_0(2), \ldots, x_0(n))$, and the comparative sequences are defined as $X_i = (x_i(1), x_i(2), \ldots, x_i(n))$, $i = 1, 2, \ldots, m$. The grey relation coefficient between X_0 and X_i at the kth datum is defined as

$$\varepsilon_{0i}(k) = \frac{\Delta_{\min} + \xi\Delta_{\max}}{\Delta_{0i}(k) + \xi\Delta_{\max}},\ k = 1, 2, \ldots, n;\ i = 1, 2, \ldots, m, \quad [1]$$

where $\Delta_{0i}(k) = |\, x_0(k) - x_i(k)\,|$, $\Delta_{\max} = \max_i \max_k \Delta_{0i}(k)$, and $\Delta_{\min} = \min_i \min_k \Delta_{0i}(k)$ for $i = 1, 2, \ldots, m$ and $\xi \in (0, 1]$. ξ is a distinguishing coefficient that controls the resolution between $\Delta_{\max}$ and $\Delta_{\min}$ (Huang *(30)*). Although ξ is an adjustable parameter according to different demands, usually ξ is set to 0.5 (Peng and Kirk *(22)*). Once all of the grey relational coefficients are determined, their weighted average, termed the grey relational grade, is computed by

$$\varepsilon_{0i} = \frac{1}{n}\sum_{k=1}^{n} \varepsilon_{0i}(k),\ i = 1, 2, \cdots, m. \quad [2]$$

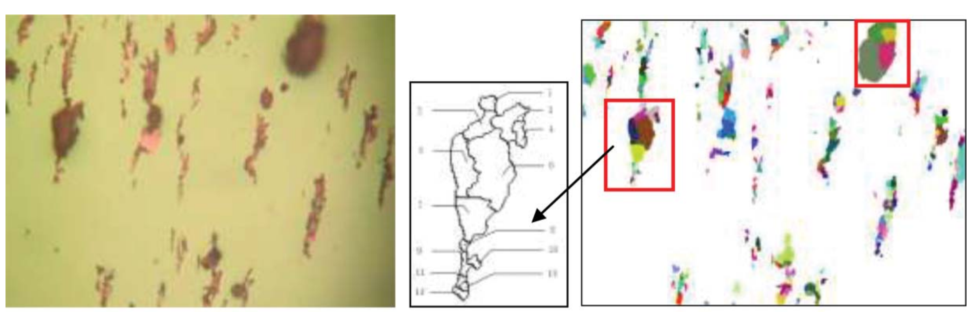

(a) (b)

Figure 4. Marker-controlled watershed segmentation: (a) original image and (b) result.

$\varepsilon_{0i} \in (0, 1]$. The larger the grey relational grade, the more similar the comparative sequence is to the reference sequence.

The modified grey clustering algorithm is based on grey relational analysis (Huang (30)). For a given data set X, the objective of cluster analysis is to analyze the similarity among data and to classify the given data set into a number of clusters, where the objects inside a cluster show a certain degree of similarity. The relational grade coefficients are used as indices that describe the relationship among the data sets and partition the data into clusters according to the correlation among them.

Assume that the m-dimensional input data are defined as $X = \{x_1, x_2, \ldots, x_m\}$, and the ith reference sequence is denoted as $x_i = \{x_i(1), x_i(2), \ldots, x_i(n)\}$, where $i = 1, 2, \ldots, m$, and each sequence has n features. The jth comparative sequence is represented as $x_j = \{x_j(1), x_j(2), \ldots, x_j(n)\}$.

For all $i, j = 1, 2, \ldots, m$, calculation of all of the grey relational grades between x_i and x_j leads to the correlation matrix:

$$A = \begin{bmatrix} \varepsilon_{11} & \varepsilon_{12} & \cdots & \varepsilon_{1m} \\ \varepsilon_{21} & \varepsilon_{22} & \cdots & \varepsilon_{2m} \\ \vdots & \vdots & \ddots & \vdots \\ \varepsilon_{m1} & \varepsilon_{m2} & \cdots & \varepsilon_{mm} \end{bmatrix}.$$

Then, for the threshold value $P_0 \in (0, 1)$, if $\varepsilon_{ij} > P_0 (i \neq j)$, x_i and x_j have high similarity and belong to the same cluster. Therefore, grey relational analysis can be viewed as a measure of similarity for finite sequences.

Under the assumption that the pixels constituting the meaningful regions (wear particles) of an image share similar feature characteristics, in the grey clustering process, color uniformity is considered a criterion for merging the neighboring regions corresponding to wear particles in the original image. Therefore, both the color information and the relative position information of each neighboring region are utilized in the grey clustering algorithm.

Color information of regions

Color image segmentation attracts increasing attention mainly because color images can provide more information than grey-level images (Cheng, et al. (31)). Color spaces including red–blue–green (RBG), hue saturation intensity (HSI), and CIELab (a color space specified by the International Commission on Illumination) have individual advantages and disadvantages. Choice of color space is still difficult in image segmentation (Cheng, et al. (31)). In our previous research, it was found that better segmentation result could be achieved by utilizing the color information in the CIElab color space (Wang, et al. (12)).

At least four parameters are required in grey modeling (Deng (32)). In the CIELab color space, L represents the lightness components and a and b are two different color components. In the RGB color space, the three color components are red, green, and blue; therefore, the six components L, a, b, R, G, and B are selected as the parameters for the grey clustering in this study.

In this article, the image after the marker-controlled watershed segmentation is divided into regions; thus, the image is defined as image $= \{X_i | i = 1, 2, \ldots, m\}$, where X_i is the ith region in the image and m is the number of regions. In each region, there are num pixels, $X_i = \{P_{ij} | j = 1, 2, \ldots, num\}$. Each pixel has six color parameters $P_{ij}(k)$, $k = 1, 2, \ldots, 6$, that represent the color features R, G, B, L, a, and b, respectively. The color features of each region is the average value of the color features of the pixels in that region and can be computed from the original image according to the formula

$$X_i(k) = \frac{\sum_{j=1}^{num} p_{ij}(k)}{num}, i = 1, 2, \ldots, m., \quad [3]$$

where $X_i(k)$, $k = 1, 2, \ldots, 6$, represent the color features R_{mean}, G_{mean}, B_{mean}, L_{mean}, a_{mean}, and b_{mean} of region X_i, respectively.

The color feature sequence of each region X_i, $i = 1, 2, \ldots, m$, is considered a reference sequence. The color features of the other regions X_j, $j = 1, 2, \ldots, m, j \neq i$, are considered comparative sequences. According to formulas [1] and [2], the grey relational grade ε'_{ij} of sequences X_i and X_j can be obtained (if $i = j$, $\varepsilon'_{ij} = 0$). Finally, the color correlation matrix A among regions is defined as

$$A = \begin{bmatrix} \varepsilon'_{11} & \varepsilon'_{12} & \cdots & \varepsilon'_{1m} \\ \varepsilon'_{21} & \varepsilon'_{22} & \cdots & \varepsilon'_{2m} \\ \vdots & \vdots & \ddots & \vdots \\ \varepsilon'_{m1} & \varepsilon'_{m2} & \cdots & \varepsilon'_{mm} \end{bmatrix}.$$

Relative position information of regions

The relative position information is used to avoid the wrong merger of two regions that have similar color features but are not neighbors in the image. The relative positional relationship parameter between two regions i and j is denoted as ε''_{ij}. If region i is adjacent to region j, $\varepsilon''_{ij} = 1$; otherwise, $\varepsilon''_{ij} = 0$. The relative position correlation matrix B among regions is constructed as

$$B = \begin{bmatrix} \varepsilon''_{11} & \varepsilon''_{12} & \cdots & \varepsilon''_{1m} \\ \varepsilon''_{21} & \varepsilon''_{22} & \cdots & \varepsilon''_{2m} \\ \vdots & \vdots & \ddots & \vdots \\ \varepsilon''_{m1} & \varepsilon''_{m2} & \cdots & \varepsilon''_{mm} \end{bmatrix}.$$

Therefore, the final interregional correlation matrix C is computed as

$$C = \begin{bmatrix} \varepsilon_{11} & \varepsilon_{12} & \cdots & \varepsilon_{1m} \\ \varepsilon_{21} & \varepsilon_{22} & \cdots & \varepsilon_{2m} \\ \vdots & \vdots & \ddots & \vdots \\ \varepsilon_{m1} & \varepsilon_{m2} & \cdots & \varepsilon_{mm} \end{bmatrix},$$

where $\varepsilon_{ij} = \varepsilon'_{ij} \times \varepsilon''_{ij}$.

Finally, the preset threshold $P_0 \in (0, 1)$ determines the merger of regions X_i and X_j. If $\varepsilon_{ij} > P_0 (i \neq j)$, adjacent regions X_i and X_j have similar properties, and the two regions are merged.

Table 1. Color features of each region.

	R_{mean}	G_{mean}	B_{mean}	L_{mean}	a_{mean}	b_{mean}
Region 1	144	104	66	182	133	148
Region 2	136	88	55	172	136	149
Region 3	153	108	73	185	134	147
Region 4	139	107	74	183	132	145
Region 5	119	83	51	167	133	148
Region 6	128	95	63	175	132	146
Region 7	117	86	54	168	132	147
Region 8	142	112	67	186	130	150
Region 9	179	134	86	201	132	149
Region 10	184	138	94	204	133	147
Region 11	152	117	72	190	130	149
Region 12	168	129	89	198	132	146
Region 13	202	168	106	218	128	150

Example of grey clustering

The wear particle shown in the red rectangle in Fig. 4 is taken as an example to show the merging process based on the proposed algorithm. After using the watershed algorithm, the particles in the left rectangle are divided into 13 regions. The color features of each region are presented in Table 1; the relative position information for each region is shown in Table 2; and the initial grey relational grade of each region calculated according to formulas [1] and [2] is listed in Table 3.

The merger of two regions depends on the merging threshold, which is used to indicate the similarity of two regions. Generally, the larger the merging threshold is, the more similar the merged regions are. A "1" indicates that two regions are exactly the same. In the proposed method, the color features of each region are the average values obtained by a statistical method. Based on the data analysis, it could be found that most relational grades of similar regions are larger than 0.9; hence, the merging threshold P_0 was set to 0.9 in this study. This means that two regions with a relational grade larger than the threshold will be merged. This process, including calculating the color features, relative position, and relational grade of each new region, is repeated until no two regions can be merged. The final merged result of Fig. 4b is shown in Fig. 5a.

Correction to the clustering based on the shape parameter of wear particles

The accurate segmentation of large wear particles can be realized by using the improved grey clustering algorithm. However,

Table 2. Relative position of each region.[a]

Region	1	2	3	4	5	6	7	8	9	10	11	12	13
1	0	1	0	0	0	0	0	0	0	0	0	0	0
2	1	0	1	0	1	1	0	0	0	0	0	0	0
3	0	1	0	1	0	1	0	0	0	0	0	0	0
4	0	0	1	0	0	0	0	0	0	0	0	0	0
5	0	1	0	0	0	1	1	0	0	0	0	0	0
6	0	1	1	0	1	0	1	0	0	0	0	0	0
7	0	0	0	0	1	1	0	1	0	0	0	0	0
8	0	0	0	0	0	0	1	0	1	0	0	0	0
9	0	0	0	0	0	0	0	1	0	1	1	0	0
10	0	0	0	0	0	0	0	0	1	0	0	0	0
11	0	0	0	0	0	0	0	0	1	0	0	1	1
12	0	0	0	0	0	0	0	0	0	0	1	0	1
13	0	0	0	0	0	0	0	0	0	0	1	1	0

[a]1 represents a neighboring region, and 0 represents a nonneighboring region.

Table 3. Initial grey relational grade of each region.

Region	1	2	3	4	5	6	7	8	9	10	11	12	13
1	0	0.92	0	0	0	0	0	0	0	0	0	0	0
2	0.92	0	0.88	0	0.94	0.94	0	0	0	0	0	0	0
3	0	0.88	0	0.96	0	0.91	0	0	0	0	0	0	0
4	0	0	0.96	0	0	0	0	0	0	0	0	0	0
5	0	0.94	0	0	0	0.92	0.98	0	0	0	0	0	0
6	0	0.94	0.91	0	0.92	0	0.93	0	0	0	0	0	0
7	0	0	0	0	0.98	0.93	0	0.86	0	0	0	0	0
8	0	0	0	0	0	0	0.86	0	0.86	0	0	0	0
9	0	0	0	0	0	0	0	0.86	0	0.96	0.9	0	0
10	0	0	0	0	0	0	0	0	0.96	0	0	0	0
11	0	0	0	0	0	0	0	0	0.9	0	0	0.91	0.8
12	0	0	0	0	0	0	0	0	0	0	0.91	0	0.85
13	0	0	0	0	0	0	0	0	0	0	0.8	0.85	0

ferrograph images may contain both particle chains and large particles. For particle chains that contain fine debris with similar features, an incorrect merger may occur in some cases, as shown in Fig. 5a. Therefore, a correction to the clustering is necessary.

There is a large difference between the shapes of wear particle chains and large particles. Wear particle chains appear elongated, whereas large wear particles such as severe sliding and fatigue particles tend to appear flaky or chunky. Therefore, the equivalent ellipse aspect ratio can be used to distinguish large wear particles from particle chains. Normally, the aspect ratio of large wear particles is 1–3.75, but it depends on the measurement method and calculation algorithm (Peng and Kirk *(22)*). Based on our statistics, in most cases, the experimental results are appropriate when the aspect ratio is set to 3.

The aspect ratio of each region obtained from grey clustering is calculated. If the aspect ratio of a region is smaller than the preset threshold, the grey clustering result is considered final; otherwise, the grey clustering result is discarded and the watershed segmentation result is retained.

Hence, the segmentation of large wear particles is obtained, and the incorrect merger of fine wear debris on deposited chains is avoided through the above process. Figure 5b shows the final result of CMWGC segmentation.

Detailed steps of the proposed algorithm

The proposed algorithm has four major steps as follows:

- Step 1: Apply a preprocessing technique such as smoothing and filtering to the original image.
- Step 2: Apply the marker-controlled watershed algorithm to the gradient image to obtain the initial segmentation. Oversegmentation may occur in some cases. The original image is segmented into m regions with each region having a special label.
- Step 3: Improved grey clustering is applied to merge the oversegmented region.
  - Step 3.1: Calculate the color parameters of each region from the original image. The initial sequences are $X_1, X_2, \ldots, X_m$ representing m regions after the watershed. Then, set the loop flag to 1.

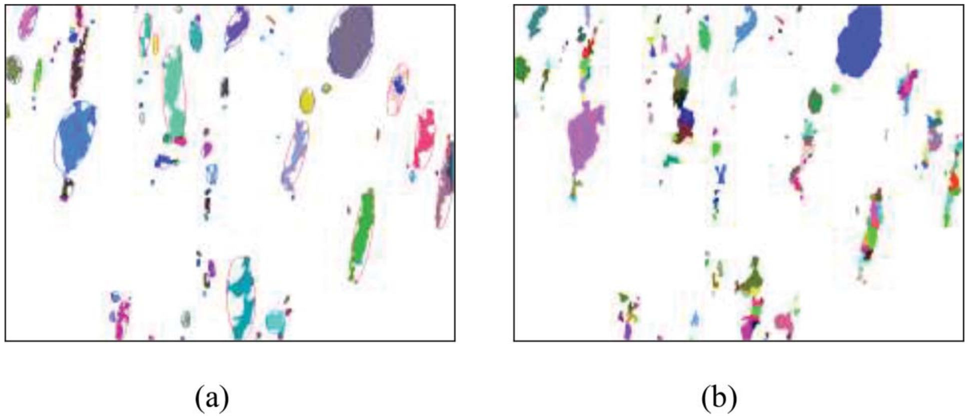

Figure 5. CMWGC segmentation: (a) clustering and (b) final result.

Step 3.2: Start the cycle. The flag is cleared. Calculate the grey relational grade ε'_{ij} of each region to obtain the color relational matrix A.

Step 3.3: Determine the relative position matrix B according to the neighboring relation of each region.

Step 3.4: Calculate $\varepsilon_{ij} = \varepsilon'_{ij} \times \varepsilon''_{ij}$ to get the relation matrix C of regions.

Step 3.5: Set the threshold $P_0 \in (0, 1)$. If $\varepsilon_{ij} > P_0 (i \neq j)$, merge region X_i with region X_j. Then set $flag = 1$.

Step 3.6: Recalculate the parameters $L_{mean}, a_{mean}, b_{mean}, R_{mean}, G_{mean}, B_{mean}$ of each region. Update each sequence and also update the labels of the reference images.

Step 3.7: Check the loop flag. If $flag = 1$, go to step 3.2; otherwise, go to the next step.

Step 4: Calculate the aspect ratio of each region to correct the clustering result.

Experimental results

Three typical ferrograph images of petrochemical equipment are selected as the experimental images. Figure 6a shows an original ferrograph image that has inconsistent background brightness. Figure 7a shows an image that has the background color in dark green with black oxide wear particles and wear particle chains. Figure 8a shows an image that has a black wear particle with blurred edges and a severe sliding wear particle with a scratch. Each image size is 800 × 600 pixels. The program of the proposed CMWGC algorithm is based on

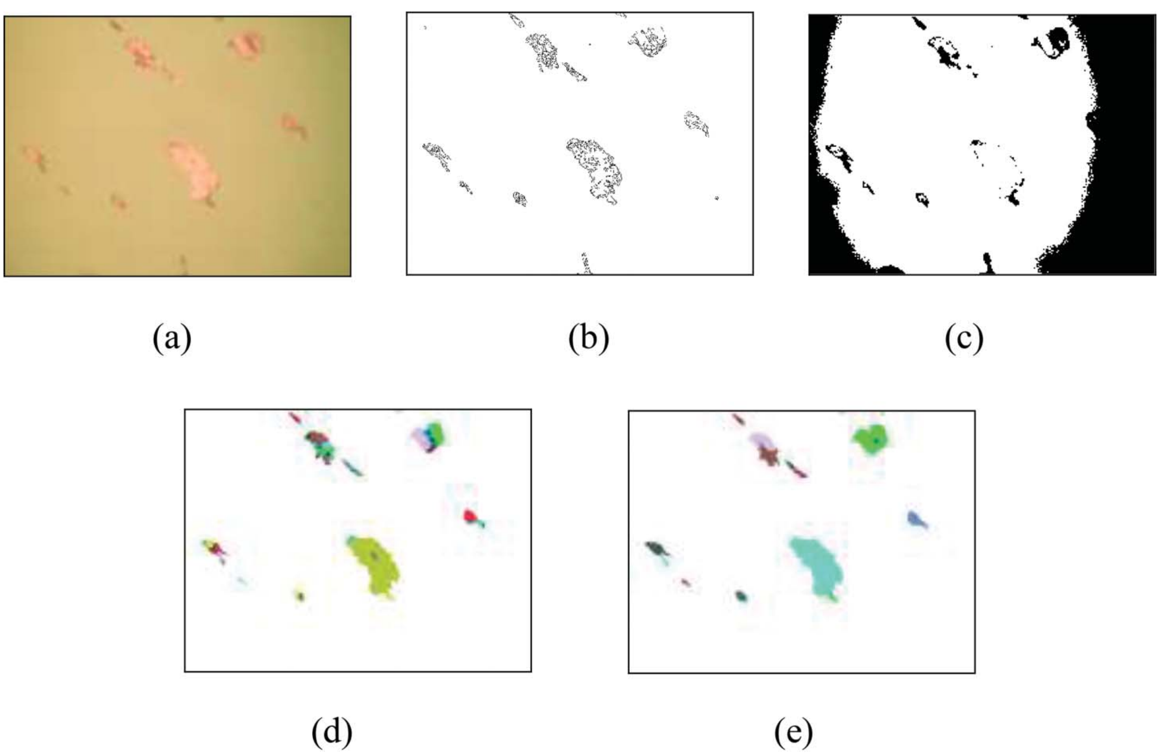

Figure 6. Segmentation results of ferrograph image example 1: (a) original image, (b) Canny, (c) Otsu, (d) marker-controlled watershed, and (e) CMWGC.

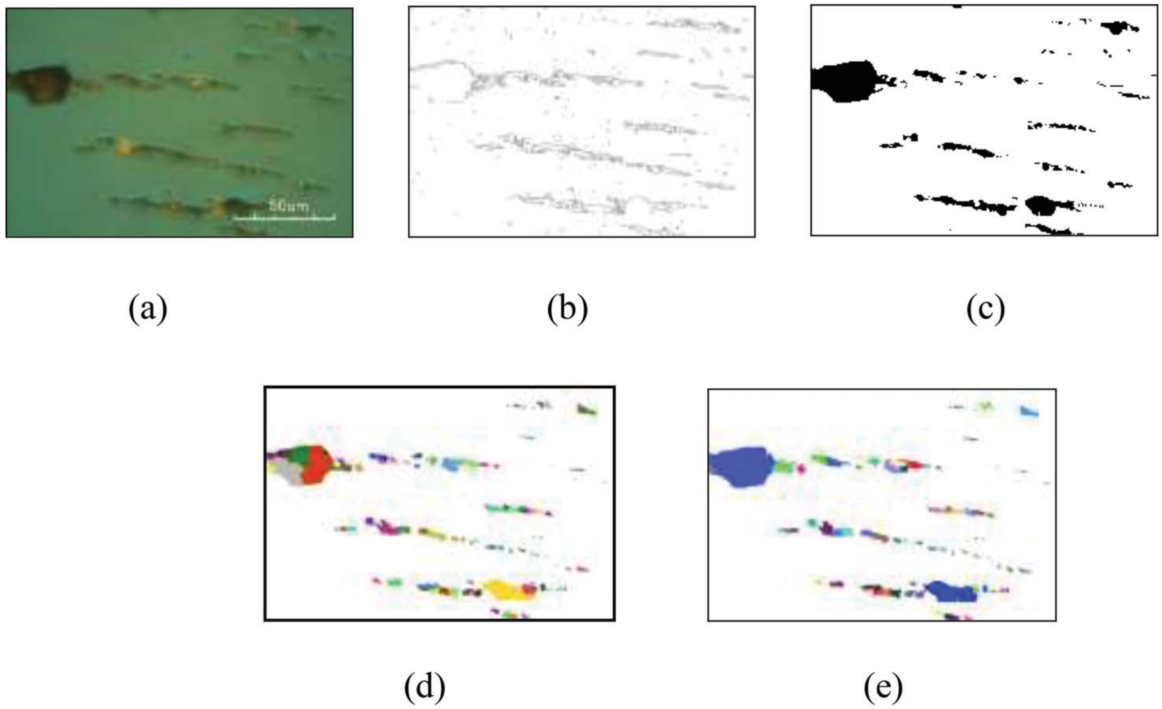

Figure 7. Segmentation results of ferrograph image example 2: (a) original image, (b) Canny, (c) Otsu, (d) marker-controlled watershed, and (e) CMWGC.

VC ++ 6.0 and OpenCV 1.0 in a 2.60 GHz i5-3230M CPU note computer.

Figures 6 to 8 show the experimental segmentation results of ferrograph images using Canny *(33)*, Otsu *(34)*, marker-controlled watershed, and the proposed CMWGC algorithm. The separated wear particles are shown in different colors.

When using the Canny edge detection algorithm, some blurred edges tend to be lost, as shown in Figs. 7b and 8b, and for particles with textures on the surfaces, Canny edge detection generated many false edges, as shown in Fig. 6b.

When using the Otsu threshold method for ferrograph image segmentation, part of the background was erroneously divided into different wear particles for regions where the background has uneven brightness, and wear particles with high brightness were sometimes mistakenly considered as background, as shown in Figs. 6c and 8c. The Otsu threshold method used a single threshold for segmenting the image into

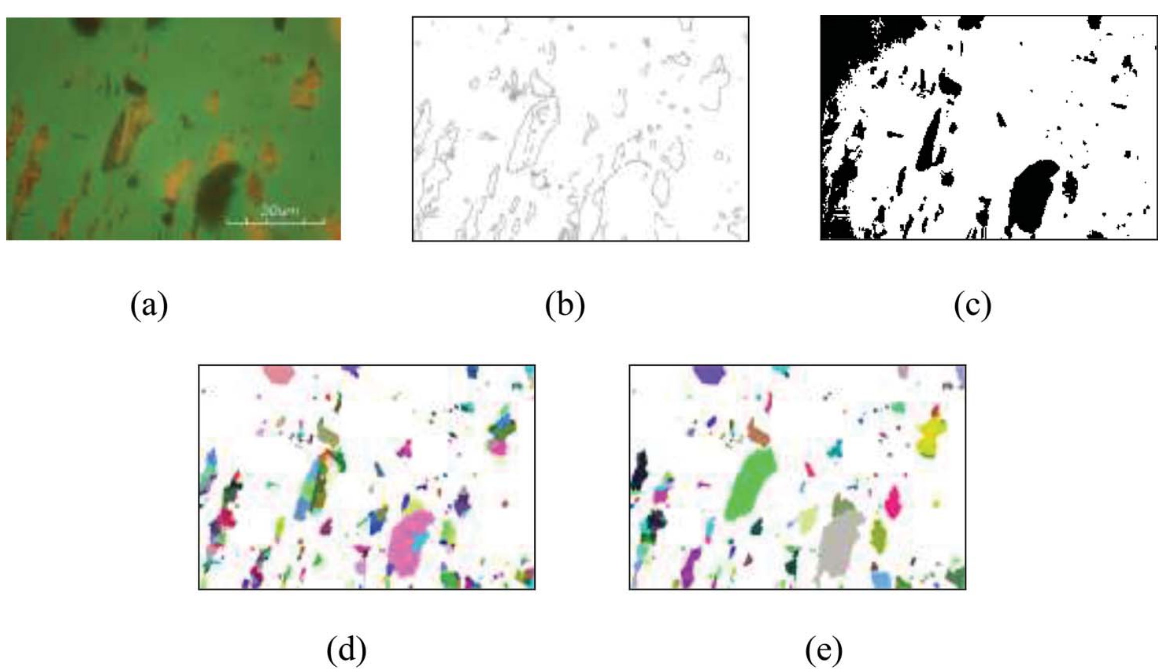

Figure 8. Segmentation results of ferrograph image example 3: (a) original image, (b) Canny, (c) Otsu, (d) marker-controlled watershed, and (e) CMWGC.

wear particles and background but was unable to achieve division between wear particles.

Because of the immersion mechanism of the watershed algorithm, the single-pixel-wide, connective, closed contours of wear particles can be obtained when the marker-controlled watershed algorithm is applied to the ferrograph images, and wear particles including those with low contrast and weak boundaries can be completely separated. However, as evidenced from Figs. 6d to 8d, certain wear particles, especially large wear particles, are mistakenly separated into fine debris.

Compared to the previous methods, the proposed CMWGC method is a hybrid method. CMWGC also takes the advantages of marker-controlled watershed, such as complete division of the image, and the advantages of the grey clustering algorithm, such as simplicity and high speed. As a result, each part of a ferrograph image is properly segmented into wear particles and background, fine wear debris on deposited chains, and large wear particles, as shown in Figs. 6e to 8e.

Conclusions

Ferrography is a useful method of determining the wear condition of machines. Wear particle segmentation is the first and critical step for intelligent ferrography based on computer image analysis. However, because the wear particles are often deposited in the form of chains, which may be composed of a number of fine wear debris and possible large wear particles, accurate segmentation of these particles is difficult. In addition, the random, complex morphology (shape, color, and surface texture) and blurred edges of wear particles lead to difficulties in computer-aided ferrograph analysis.

In this article, a new method that combines the marker-controlled watershed and grey clustering algorithm is proposed for the segmentation of ferrograph images. Applying the marker-controlled watershed transform on the gradient image sets an initial partitioning of the image into primitive regions. This step presents each region with closed and single-pixel-width contours and edges. Then, this initial partition is the input to a grey clustering process to overcome the inherent problem of watershed segmentation—that is, oversegmentation. Finally, the identification and correction algorithm based on prior knowledge, such as the aspect ratio of wear particles, is applied to produce the final segmentation. To demonstrate the effectiveness of the proposed method, several examples have been provided. In each example, the performance of the proposed algorithm was compared with that of the Canny, Otsu, and marker-controlled watershed methods. Experimental results show that the proposed approach outperformed the others and is a practical method to segment wear particles quickly and efficiently.

Funding

This research is supported by the National Natural Science Foundation of China (No. 51205202).

References

(1) Roylance, B. J. (2005), “Ferrography—Then and Now,” *Tribology International*, **38**(10), pp 857–862.
(2) Laghari, M. S., Memon, Q. A., and Khuwaja, G. A. (2004), “Knowledge Based Wear Particle Analysis,” *International Journal of Information Technology*, **1**(3), pp 91–95.
(3) Wu, T., Wang, J., Peng, Y., and Zhang, Y. (2012), “Description of Wear Debris from On-Line Ferrograph Images by Their Statistical Color,” *Tribology Transactions*, **55**(5), pp 606–614.
(4) Eliaz, N., and Latanision, R. (2007), “Preventative Maintenance and Failure Analysis of Aircraft Components,” *Corrosion Reviews*, **25**(1–2), pp 107–144.
(5) Cao, W., Chen, W., Dong, G., Wu, J., and Xie, Y. (2014), “Wear Condition Monitoring and Working Pattern Recognition of Piston Rings and Cylinder Liners Using On-Line Visual Ferrograph,” *Tribology Transactions*, **57**(4), pp 690–699.
(6) Zhang, Y., Mao, J., and Xie, Y. (2011), “Engine Wear Monitoring with OLVF,” *Tribology Transactions*, **54**(2), pp 201–207.
(7) Peng, Z., and Goodwin, S. (2001), “Wear-Debris Analysis in Expert Systems,” *Tribology Letters*, **11**(3–4), pp 177–184.
(8) Wang, J., and Wang, X. (2013), “A Wear Particle Identification Method by Combining Principal Component Analysis and Grey Relational Analysis,” *Wear*, **304**, pp 96–102.
(9) Stachowiak, G. P., Stachowiak, G. W., and Podsiadlo, P. (2008), “Automated Classification of Wear Particles Based on Their Surface Texture and Shape Features,” *Tribology International*, **41**(1), pp 34–43.
(10) Stachowiak, G. W., and Podsiadlo, P. (2006), “Towards the Development of an Automated Wear Particle Classification System,” *Tribology International*, **39**(12), pp 1615–1623.
(11) Surapol, R. (2005), “Wear Particle Analysis—Utilization of Quantitative Computer Image Analysis: A Review,” *Tribology International*, **38**(10), pp 871–878.
(12) Wang, J., Zhang, L., and Wang, X. (2013), “Combining *k*-Means Clustering and Watershed Algorithm for the Segmentation of Color Ferrograph Image,” *Journal of China University of Mining & Technology*, **42**(5), pp 866–872.
(13) Wu, T., Wu, H., Du, Y., Kwok, N., and Peng, Z. (2014), “Imaged Wear Debris Separation for On-Line Monitoring Using Gray Level and Integrated Morphological Features,” *Wear*, **316**(1–2), pp 19–29.
(14) Peng, Z. (2002), “An Integrated Intelligence System for Wear Debris Analysis,” *Wear*, **252**, pp 730–743.
(15) Vincent, L., and Soille, P. (1991), “Watersheds in Digital Spaces: An Efficient Algorithm Based on Immersion Simulations,” *IEEE Transactions on Pattern Analysis and Machine Intelligence*, **13**(6), pp 583–598.
(16) Nallaperumal, K., Krishnaveni, K., Varghese, J., Saudia, S., and Annam, P. K. (2007), “A Novel Multi-Scale Morphological Watershed Segmentation Algorithm,” *International Journal of Imaging Science and Engineering*, **1**(2), pp 60–64.
(17) Grau, V., Mewes, A. U. J., Alcañiz, M., Kikinis, R., and Warfield, S. K. (2004), “Improved Watershed Transform for Medical Image Segmentation Using Prior Information,” *IEEE Transactions on Medical Imaging*, **23**(4), pp 447–458.
(18) Yang, W., Guo, L., Zhao, T., and Xiao, G. (2008), “Image Segmentation Method Based on Watersheds and Ant Colony Clustering,” *Chinese Journal of Quantum Electron*, **25**(1), pp 19–24.
(19) Monteiro, F. C. (2008), “Watershed Framework to Region-Based Image Segmentation,” *19th International Conference on Pattern Recognition*, ICPR 2008, Tampa, FL, USA, December 8–11, 2008, pp 1586–1589.
(20) Wang, J., Zhang, L., Lu, F., and Wang, X. (2014), “The Segmentation of Wear Particles in Ferrograph Images Based on an Improved Ant Colony Algorithm,” *Wear*, **311**(1–2), pp 123–129.
(21) Deng, J. (1982), “Control Problems of Grey System,” *System and Control Letters*, **1**(5), pp 288–294.
(22) Peng, Z., and Kirk, T. B. (1999), “Wear Particle Classification in a Fuzzy Grey System,” *Wear*, **225–229**, pp 1238–1247.
(23) Chen, S., Li, Z., and Xu, Q. (2006), “Grey Target Theory Based Equipment Condition Monitoring and Wear Mode Recognition,” *Wear*, **260**, pp 438–449.

(24) Huang, H. C., and Wu, J. L. (1993), "Grey System Theory on Image Processing and Lossless Data Compression for HD-Media," *The Journal of Grey System Theory and Practice*, **3**(2), pp 9–15.

(25) Feng, D., Zhang, B., and Wang, X. (2009), "A Novel Operator Based on Grey Relational Analysis," *4th IEEE Conference on Industrial Electronics and Applications*, ICIEA 2009, Xi'an, China, May 25–27, 2009, pp 2686–2689.

(26) Ma, M., Jiao, L., and He, Z. (2009), "Grey Clustering Analysis Based Performance Evaluation on Image Segmentation," *2009 International Conference on Test and Measurement* (ICTM 2009), Hong Kong, China, December 5–6, 2009, pp 14–17.

(27) He, R., Huang, D., and Chen, J. (2005), "Image Edge Detection Based on Grey Prediction Model," *Journal of Northwestern Polytechnical University*, **23**(1), pp 15–18.

(28) Vincent, L. (1993), "Morphological Gray Scale Reconstruction in Image Analysis: Applications and Efficient Algorithms," *IEEE Transactions on Image Processing*, **2**(2), pp 176–201.

(29) Chang, K. C., and Yeh, M. F. (2005), "Grey Relational Analysis Based Approach for Data Clustering," *IEE Proceedings - Vision, Image, and Signal Processing*, **152**(2), pp 165–172.

(30) Huang, K. Y. (2008), "An Auto-Recognizing System for Dice Games Using a modified Unsupervised Grey Clustering Algorithm," *Sensors*, **8**, pp 1212–1221.

(31) Cheng, H. D., Jiang, X. H., Sun, Y., and Wang, J. (2000), "Color Image Segmentation: Advances and Prospect," *Pattern Recognition*, **34**, pp 2259–2281.

(32) Deng, J. (1989), "Introduction to Grey System Theory," *The Journal of Grey System Theory and Practice*, **1**(1), pp 1–24.

(33) Canny, J. F. (1986) "A Computational Approach to Edge Detection," *IEEE Transactions on Pattern Analysis and Machine Intelligence*, **8**(6), pp 689–698.

(34) Otsu, N. (1979) "A Threshold Selection Method from Gray Level Histograms," *IEEE Transactions on Systems, Man, and Cybernetics*, **9**(1), pp 62–69.